Steel and Composite Structures, *Vol. 34, No. 6 (2020) 891-907*
DOI: https://doi.org/10.12989/scs.2020.34.6.891

Experimental study on hysteretic behavior of steel moment frame equipped with elliptical brace

Habib Ghasemi Jouneghani[a] and Abbas Haghollahi*

Department of Civil Engineering, Faculty of Civil Engineering, Shahid Rajaee Teacher Training University, Tehran, Iran

(*Received July 29, 2019, Revised October 16, 2019, Accepted February 18, 2020*)

Abstract. Many studies reveal that during destructive earthquakes, most of the structures enter the inelastic phase. The amount of hysteretic energy in a structure is considered as an important criterion in structure design and an important indicator for the degree of its damage or vulnerability. The hysteretic energy value wasted after the structure yields is the most important component of the energy equation that affects the structures system damage thereof. Controlling this value of energy leads to controlling the structure behavior. Here, for the first time, the hysteretic behavior and energy dissipation capacity are assessed at presence of elliptical braced resisting frames (ELBRFs), through an experimental study and numerical analysis of FEM. The ELBRFs are of lateral load systems, when located in the middle bay of the frame and connected properly to the beams and columns, in addition to improving the structural behavior, do not have the problem of architectural space in the bracing systems. The energy dissipation capacity is assessed in four frames of small single-story single-bay ELBRFs at ½ scale with different accessories, and compared with SMRF and X-bracing systems. The frames are analyzed through a nonlinear FEM and a quasi-static cyclic loading. The performance features here consist of hysteresis behavior, plasticity factor, energy dissipation, resistance and stiffness variation, shear strength and Von-Mises stress distribution. The test results indicate that the good behavior of the elliptical bracing resisting frame improves strength, stiffness, ductility and dissipated energy capacity in a significant manner.

Keywords: innovative elliptic bracing system; energy dissipation; hysteretic behavior; experimental behavior; seismic performance

1. Introduction

The structure behavior during seismic events is assessed according to the encountered losses. High dependency to hysteretic energy on structural damage has led this concept to be considered in modern structural design methods (Kazantzi *et al*. 2014, Fanaie *et al*. 2014, 2016). In these methods, the given design is based on the fact that the elastic vibration which makes the structural deformation merely transfers energy input by ground motion into kinetic energy which is partially dissipated by damping and the rest shall make the structure vibration continually. The basic principle in this method is the optimal distribution of damage and the proper distribution of resistance in structures (Shin *et al*. 2016, Khatamirad *et al.* 2017, Abdollahzadeh *et al*. 2018).

Inappropriate behavior of the structures against earthquakes has led to proposal of an energy-based approach in designing seismic-resisted structures. Plastic design concepts and an energy equilibrium equation are applied in either designing or modifying the moment resistant frame members (Bojórquez *et al*. 2015, Sultana and Youssef 2016). In the researcher’s view, hysteretic energy demand due to inelastic deformation is considered as a key parameter in design together with structural behavior (Fanaie *et al.* 2017, Xue *et al* 2009). Based on this view, many analytical methods and strategies have been and are being proposed to simulate the structures’ behavior (Sahoo and Chao 2010, Speicher and Harris 2016, Kaveh *et al.* 2010, Fanaie and Shamlou 2015).

For the first time Housner (1956) proposed an energy-based design, where the capacity of structures to absorb energy from big earthquakes is considered as a safety factor for structures. To him, the portion of seismic energy value released on a structure is equal to the mass movement and a removable transformation of the members of the structure. This energy is dissipated parts though yielding, inelastic deformations and damping in structural members. Structures must be designed and constructed in a sense that they can absorb and dissipate the highest value of released energy with minimal damage to the structure (Doğru *et al.* 2017, Baat and Bayat 2014). Absorbing seismic energy and damage models thereof for single-degree-of-freedom systems (SDOF) are studied by Wu and Hanson (1989).

Due to the obvious advantages, BRBs have been extensively studied and widely used in engineering practices recently. It is capable of providing the rigidity needed to satisfy structural drift limits, while delivering a substantial and repeatable energy dissipation capability (Black *et al*. 2004). What’s more, the self-centering brace combining a frictional energy dissipation mechanism and

*Corresponding author, Assistant Professor
E-mail: Haghollahi@Sru.ac.ir
[a]Ph.D. Candidate
E-mail: Ghasemi@Sru.ac.ir

http://www.techno-press.org/?journal=scs&subpage=6
ISSN: 1229-9367 (Print), 1598-6233 (Online)

aramid tension elements have first proposed by Christopoulos *et al.* (2008). Xu *et al*. (2017, 2018) proposed a pre-pressed spring self-centering friction brace with repeatable flag-shaped hysteretic behavior, a self-centering variable/constant damping brace to get a hysteretic response. Both these two types of the braces can avoid out-of-plane buckling.

Zahrah and Hall (1984) assessed the important and effective parameters for the absorbance of earthquake energy in SDOF structures, the nonlinear response of simple structures and the potential for damage due to earthquake movement. To them, the effective value of movement could be determined based on the value of energy released in the structures. The equivalent plastic cycles as important feature in seismic design are obtained based on wasted energy, by considering the input energy as an appropriate basis for a designed earthquake selection. By Uang and Bertero (1998) energy is a reliable parameter to define the potential for damage from an earthquake. Léger and Dussault (1992) assessed the influence of many mathematical models of different damping's on the destruction of seismic energy from MDOF structures in a parametric manner. Housner and Jennings (1977) and Kuwamura and Galambos (1989) claimed that a structure can withstand severe seismic forces, if the energy absorption capacity of the structure is greater than the seismic input energy.

Geol and Berg (1968) assessed the distribution of energy in asymmetric structures and found that the released energy to the symmetric and asymmetric single-story structures is similar. They revealed that in an asymmetric structure, hysteretic energy demand for stiff elements is the same as its initial value, while the same demand is higher for malleable elements. Kunnath and Chai (2004) provided an acceptable passage that converts the released energy in to the wasted energy of the system. They defined a spectrum for several periodical inelastic loads of a structure based on hysteretic energy that describes experimental damage potentially caused by the earth movement. Benavent (2007) defined a model to determine the damage to components of steel structures with stable hysteresis behavior against earthquakes. The damage considered in this model is a combination of general hysteretic energy as the maximum inter-story drift. Damage to this model is defined with two parameters of general hysteretic energy and the general wasted energy at the skeleton as to the force and the inter-story drift curve. Cao and Friswell (2009) assessed the effect of the earthquake energy concentration on the inelastic response of reinforced concrete structures and found that the greatest concentration of energy is observed during the main period of the structure.

Although, there exist many uncertainties in scientific justification and performance of energy parameters which prevent devising a legal method accordingly, their application as a preliminary seismic design is proven. By applying the energy method in designing earthquake-resisting structures the proper seismic capacity and requirement are estimated. Understanding this need for structures is related to the type of structural system in building design. The seismic systems like moment resisting frame (MRF) and concentric bracing frame (CBF) have long been applied in steel structures because their stiffness and ductility constitute the two important factors affecting the seismic response of a structure, while both the systems do not have stiffness and ductility simultaneously. CBFs are of good stiffness, but inappropriate ductility and MRFs are of low stiffness with acceptable ductility. For most of structures, including those two, MRF and CBF, of course possess/have the capacity simultaneously, though the stiffness and ductility may be great or small. Although the MRF system is a good energy dissipating system, its large cross sections are not cost-effective.

The eccentric bracing frame and knee braced frame are proposed by Roeder and Popov (1978a) and Aristizabal-Ochoa (1986), respectively. Bond beam in the eccentric bracing frame, and the knee element in the knee braced frame as the ductile fuses of the system are responsible for dissipating released energy from the earthquake through yielding in shear and bending. By applying the capacity-based design concept, other frame components (including the diagonal member, beam, and column) are designed by each one of the fuses mentioned above for the expected capacity to assure the functionality of these components in the inelastic area. Engelhardt and Popov (1989) run an experimental study on eccentric bracing frame structures with a tall bond beam connected to the column in order to asserts the probable instabilities of the beam part outside the bond beam and to understand the current mechanisms in the tall bond beams. Okazaki *et al.* (2004) run 23 experiments to study the performance of bond beams in eccentric bracing frames resistant to earthquake subject to alternative loading. Richards and Uang (2005) assessed the effect of flange width to thickness ratio on the performance of bond beams through FEM. Richards and Uang (2006) proposed a modified loading protocol for obtaining the performance of the bond beam against actual earthquakes in a rational manner. Mofid and Khosravi (2000) revealed that the nonlinear behavior of the knee brace subject to lateral loads in the bending and shear yielding modes depends on its configuration. One of the important views in designing structures is its behavior against earthquake lateral loads in order to increase rigidity, stability and energy dissipation.

Attempt is made in this article to propose an innovative bracing system, where the stiffness, ductility, and productivity increase only by changing the geometry of the brace. An elliptic bracing resisting frame is a new type of frame with high energy dissipation properties with applying the advantage of the SMRF system (energy dissipation and ductility) and the X-bracing system (good stiffness). These new ELBRFs systems do not have the problem of repairing beams in EBF and the problem of repairing column in the Knee braces, while the main components of the structure (beam and column) remain safe because the plastic hinges are confined in the elliptic bracing. Accordingly, elliptic bracing, as a structural fuse of the frame, it becomes damaged during a severe earthquake, by preventing any failure in the main components. This justifies the repair of elliptic bracing instead of the frame, thus its cost effectiveness.

A good lateral stiffness can be obtained by implementing the connections in the elliptic bracing in a proper manner. Unlike other bracing systems, applying these systems in addition to improving structural stiffness and ductility, the designer can install it in any part of the structure without any interference with architectural space.

In Architectural Context, this system can be viewed as an appropriate member. As the lateral load increases, the geometry of the structure changes so that the elliptic bracing form contributes to a rapid change in the internal force of the bracing from tension to compression and vice versa at the moment of shifting the lateral load direction. The behavior of the elliptic bracing system is geometrically nonlinear and has high ductility and proper stiffness. The geometric form of this bracing in more energy dissipation than the lateral force, and as a ductile fuse, it increases the system ductility.

Elliptical brace is made in different forms of: 1) with and without steel brackets and 2) with fillers in the corners of the frame. This system can be installed in in-situ middle bays either to cover one bay, Fig. 1 or to cover multi bays, Fig. 2, according to the structure design.

The advantages of these new ELBRFs systems are briefed as follows:

1- elliptic brace can be pre-manufactured at a workshop, and its connection to the in-situ middle bay of the frame is easy, so its time and the cost of construction are reduced

2- significant resistance and ideal lateral stiffness can be applied freely by adding steel bracket or filling corners with steel plates

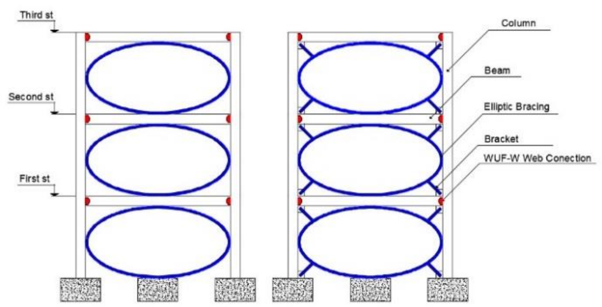

Fig. 1 ELBRFs bracing system in mid height buildings

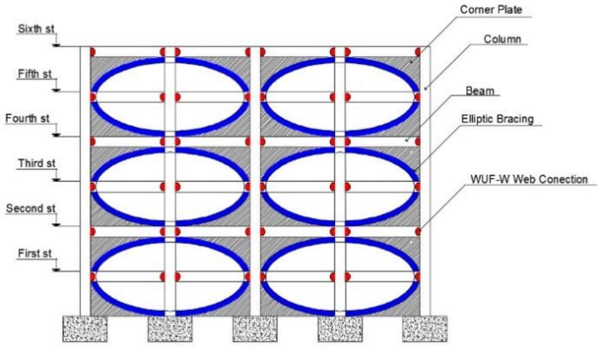

Fig. 2 ELBRFs bracing system in tall buildings

3- the position of these systems in the facade of the building exhibits appropriate opening

4- elliptic bracing can be initially applied subject to lateral loads to dissipate energy and protect the main members of the structure from serious damage

The objective here is to introduce innovative ELBRFs systems, endowed with a combination of high ductility and energy dissipation capacity from SMRF and a high elastic stiffness from CBF, and to assess the hysteretic performance of a structural. For this purpose, the capacity of four frames of a small single story ELBRFs, at ½ scale, and different shapes, through a series of cyclic tests are assessed and compared with SMRF and X- bracing systems. Verification of the finite element of all frames is confirmed by comparing the experimental results, in order to determine the analytical and numerical shear strength of the ELBRFs systems; to compare seismic behavior and performance of all these systems with respect to failure modes, hysteresis loops, stiffness, resistance, ductility, Von-Mises stress distribution, deformation and energy dissipation capacity and to study the seismic needs as a design criterion in ELBRFs structures.

2. Hysteretic energy

One of the practical implications in the seismic design of structures is to adopt the concept of earthquake-related damages in structures to provide sufficient security for the physical safety and to determine the structural damage value and its reduction. The structure and earthquake behaviors and their interaction are essential to determine the potential for damage, (Taniguchi and Takewaki 2015, Khaloo *et al.* 2016, Abdollahzadeh and Faghihmaleki 2016).

If the seismic design of structures to be consistent with the concepts of energy is sought, the potential for damage in a similar manner should be of concern, (Aguirre and Almazán 2015). Studies reveal that the energy released in the structure, is partly dissipated in damping and hysteretic energies (elastic behavior) forms and the remainder is stored as kinetic and strain energies. The structural energy equilibrium is expressed as follows

$$E_{\text{inter}} = E_k + \left(E_s + E_h\right) + E_\xi \Rightarrow \\ -\int m\ddot{u}du_g = \frac{1}{2}m\dot{u}_t^{\,2} + \int f_s du + \int C\dot{u}_t^{\,2}dt \tag{1}$$

where, E_{inter} is the inter energy; E_k is the kinetic energy; E_s is the strain energy; E_ξ is the damping energy, E_h is hysteresis energy, m is the structure mass, c is the damping coefficient, f_S is the restoring force, u is the mass displacement, $\dot{u}$ is the mass velocity, $\ddot{u}$ is the mass acceleration, u_g is the foundation displacement, and t is the time.

Hysteretic energy in a structure is an indicator of its damage level or its vulnerability, but it cannot represent the distribution of damage in its parts, the process of yielding or collapse. The distribution of energy in the structure follows

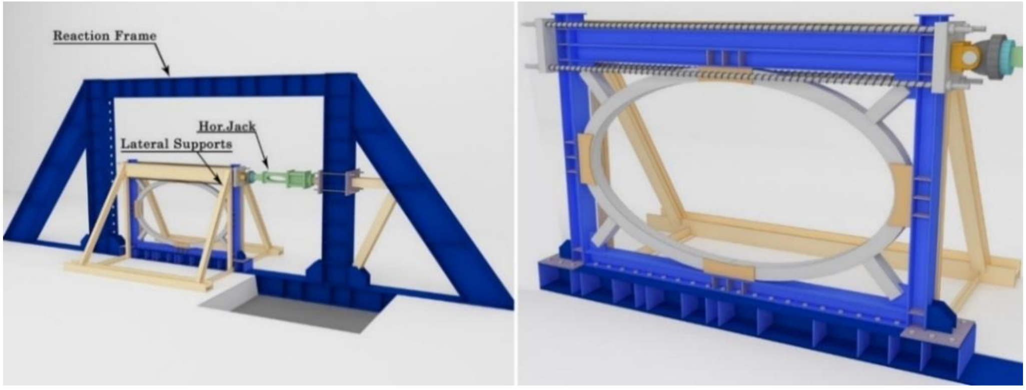

Fig. 3 A view of the test set-up in specimen ELBRF-B

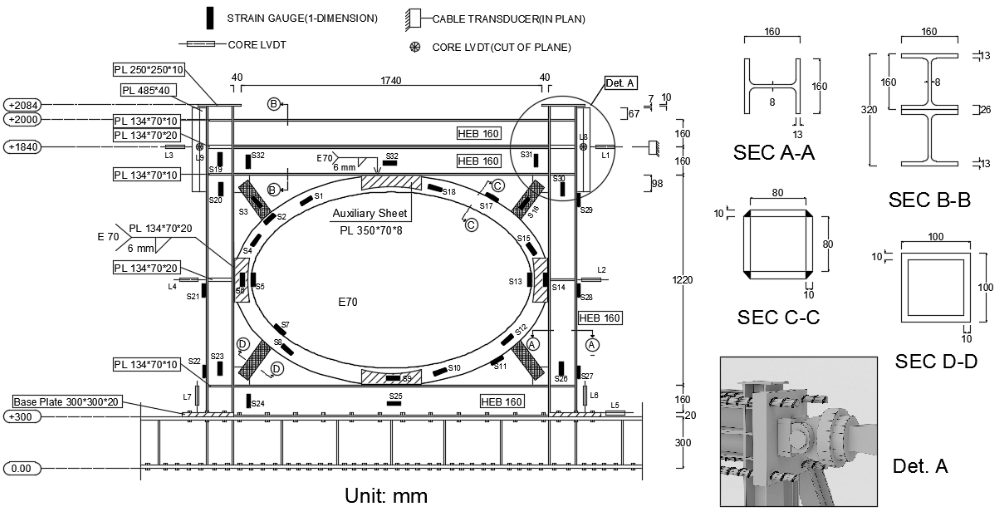

Fig. 4 Dimensional coordinates of ELBRF-B specimen set-up and the dimension of auxiliary plates

the structural model and its characteristics (López-Barraza *et al.* 2016).

3. The ELBRFs frames and their test set-up

The Experiments studies are carried out on 2D innovative elliptic bracing resistant frames, as single-story single-bay ELBRFs, in the different forms at ½ scale in the laboratory SRTTU (Tehran-Iran). The lab is equipped with an in-situ steel reaction frame within which the subject frames are to be loaded together with a stiffer base stronger than the specimens. Two steel Λ-frames are installed on either side of the subject specimens to prevent frame destruction. Horizontal loads are applied through a 2500 kN hydraulic jack as a quasi-static cyclic loading model in a completely inverse manner as to the ATC-24 protocol (1992). The images of this proposed ELBRF-B set-up and the connections to the horizontal jack are drowned in Fig. 3.

3.1 Test plan

To study the hysteretic behavior, six specimens of a 2D single-story single-bay frame are designed and built consisting of four new ELBRFs, one concentric bracing frame (X-bracing) and one SMRF as the benchmark, with a bay of 2 *m* wide and 1.5 *m* height representing the dimensions of the rectangular bay of a steel braced frame in the building, at 4 *m* wide and 3 *m* height bay. The boundary elements of the beams and columns of the subject specimens are made of HEB. Beam to column connections here is subject to welded unreinforced flange-welded (WUF-W) web connections (FEMA.350 2001) according to the American Institute of Steel Construction (AISC 360-10 2010) in order to assure the necessary ductility. Electrode E7018 is applied in all connections. An additional HEB beam is welded on the upper beam of the subject specimens to increase rigidity of the upper beam, to better control the internal forces of the panel, and to improve load transfer, Fig. 4. This method is assessed by Lubell (1997), where a good performance of the frame is recorded. To connect the two ends of the frame through the two end plates, one with a 40 *mm* thickness and the other with a 60 *mm* thickness, four Φ 36 *mm* tensile bars are applied. The purpose of addition this bar is to have a uniform tensile and compression load distribution.

Fig. 5 ELBRF-E specimen

Fig. 6 ELBRF-B specimen

The assessments run on the six specimens together with their schemes are explained as follows:

The first ELBRF-E specimen sample is designed and manufactured as a reference frame, which is a SMRF containing an elliptic bracing. The lateral stiffness of this system is provided through the elliptic brace, and the energy dissipation is produced due to the axial force generated in the elliptic brace over the seismic reciprocating force. In the lower axis of this specimen, a beam is attached for connection to the concrete foundation. The elliptic section is of manually made Tube-Box shape. To connect the elliptic braces to the beams and columns, four auxiliary plates are welded to the four connection points of the elliptic brace to the frame, Fig. 5. The reason for applying Tube-Box shape section is to obtain a perfectly precise form in making the bracing and to have precise curvatures (i.e., the large and small quadrants of the elliptic system) together with reduced residual stresses.

The second ELBRF-B resembles the first specimen, but here the four empty corners of the frame are welded to the elliptic system through four brackets, Fig. 6.

In tall and heavy structures with a larger lateral force, one of the proposed forms of the ELBRFs is the elliptical bracing frame with fillers in the corners. To increase the shear strength of this new ELBRF bracing system in these structures there exist three approaches: 1) increasing the thickness of the web plate in the columns, 2) increasing the length of the frame bay and 3) applying fillers in the frame corners. In the first approach, the value of stresses increases on the boundary elements, which in turn leads to the brittle fracture of the columns. Therefore, it is impossible to use the total capacity of the web plates, which is another disadvantage of the first approach. In the second approach, given the condition of the elliptical bracing placement in the rectangular frame bay, the frame bay length to the story height ratio is maintained within 1.33 and 1.5. The third approach can be considered as the best in increasing ELBRFs shear strength.

The third and fourth ELBRFs' specimens, (ELBRF-1 and ELBEF-2) are of the same form with the only difference in their corner plate thickness of 6 and 8 *mm*, respectively. A diagonal stiffener of 120×40×5 *mm* is welded in the middle of the triangle plate, on both sides, Figs. 7 and 8.

The specimens 5 and 6 consist of SMRF and X-bracing systems for the purpose of comparing and assessing the seismic behavior and seismic performance of ELBRFs bracing systems in a more precise sense, Figs. 9 and 10.

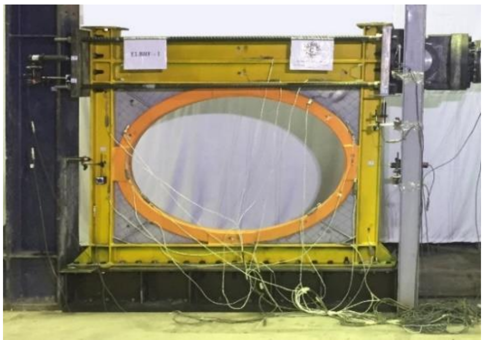

Fig. 7 ELBRF-1 specimen.

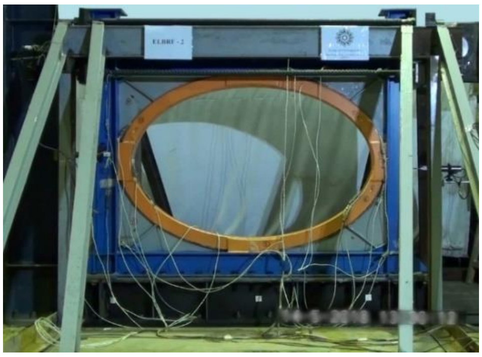

Fig. 8 ELBRF-2 specimen.

Fig. 9 SMRF specimen.

Fig. 10 X-Bracing specimen

Table 1 Details of specimens, (unit: mm)

Specimen	Beam	Column	Brace	Corner Plate	Bracket	Corner stiffener
SMRF	HEB 160	HEB 180	-------	-------	-------	-------
X-bracing	HEB 180	HEB 180	BOX 120×12	-------	-------	-------
ELBRF-E	HEB 160	HEB 160	BOX 100×10	-------	-------	-------
ELBRF-B	HEB 160	HEB 160	BOX 100×10	-------	BOX 100×10	-------
ELBRF-1	HEB 160	HEB 160	BOX 100×10	Thk. = 8	-------	PL 120×40×5
ELBRF-2	HEB 160	HEB 160	BOX 100×10	Thk. = 6	-------	PL 120×40×5

Table 2 Material Mechanical Properties of steel materials from the tension coupon tests

Steel materials	Elastic modulus (GPa)	Static yield (MPa)	Static ultimate (MPa)	Yield strain (%)	Hardening strain (%)	Ultimate strain (%)	Rupture strain (%)	Fye (MPa)	Fue (MPa)
HEB 180	204.3	360	520	0.19	1.92	24.6	22.1	432	624
HEB 160	203.2	355	512	0.17	1.86	25.0	25.4	426	614
BOX 100×10 (X-Bracing)	202.4	285	500	0.14	0.35	22.3	26.2	356	625
BOX 100×10 (ELBRFs)	205.6	360	551	0.18	3.28	20.0	20.0	414	634
Plate (Thk. = 5 mm)	205.0	340	470	0.17	2.95	20.5	22.3	391	541
Plate (Thk. = 6 mm)	205.0	310	510	0.15	2.87	21.6	24.1	357	587
Plate (Thk. = 8 mm)	204.0	283	510	0.14	0.3	21.6	27.0	325	587
Plate (Thk. = 10 mm)	205.6	360	551	0.18	2.44	20.0	19.7	414	634
Plate (Thk. = 20 mm)	202.3	340	470	0.17	3.06	20.5	22.3	391	541

The details of the six subject specimens are tabulated in Table 1. The mechanical properties of materials are tested according to ASTM A370-05 (2005) to determine theirmonotonic features of stress-strain before the frames' testing, Table 2.

The lower boundary of the material features and the expected resistance properties are considered for the force-control action and deformation-control action based on FEMA-356 (2000). The expected resistance of the material is obtained by multiplying the values of the lower boundary in the appropriate *Ry* coefficient in accordance with $F_{ye}=R_yF_y$ and $F_{ue}=R_yF_u$, equations, where, F_y, F_u, F_{ye} and F_{ue} are the lower boundary of yield resistance, lower boundary of ultimate resistance, expected yield resistance, and ultimate strength, respectively. In accordance with FEMA-356 (2000), the R_y coefficients for H-shaped sections, the sections made from the sheet and the square tube are 1.2, 1.15, and 1.25, respectively. Here, the beams and columns, the standard sections of HEB are applied and for elliptic braces, section box-tube is made of plane sheet, and for X-brace, the standard section of square tubes are applied.

3.2 Test Set-up

This experimental study is run with the objective to obtain hysteretic performance and assessing seismic behavior in this innovative ELBRFs bracing system. As observed in Fig. 3, a hydraulic actuator is applied to load the horizontal reciprocating cycles over the column. In this test, the maximum stroke is adjusted at ±200 *mm*, where the positive (+) and negative (-) signs are to apply compressive strength and tensile strength, respectively. A 2000 kN load cell records the loading cycles to measure the tensile and compressive strengths. A strong beam is installed between the strong base and the base plate of the specimens to provide a more robust and precise connections between the two bases and rise the frames to the desired height. Two Λ-frame lateral supports are designed and set on both sides of the specimens. Lateral supports do not have any mechanical connection to the specimens because they do not prevent the movement of specimens inside the loading plane. The contact surfaces between the lateral supports and the frames are lubricated to keep the frames inside the plane against any distortion.

For any specimen, a determined count of Linear Variable Differential Transformers (LVDTs) are applied to measure displacements and deformations in the reciprocating motion direction in different points of the frame, and to measure the base plate movements and control the restraint of base connections. These LVDTs are installed at different points of the frame to determine the out-of-plane displacements, and assure the consistency of the specimen inside the plane during the test. Strain gauges are connected to different points of the beams, columns, and panels and critical points of the elliptical brace. To record strength values, displacement and strain rates, an electronic data channel system is applied. The location of installing strain gauges in potential plastic areas in elements is determined based on the results of the initial numerical analysis. All specimens are painted to exhibit the post-yield points, when the paint is scaled during the test. The subject specimens before the test are shown is Figs. 5-10.

3.3 WUF–W Web connections

As illustrated in Fig. 11, the FEMA-350 (2001) is observed in applying WUF-W welded for beam column connections. The descriptions of the numerical sequence observed in Fig. 11 are expressed in Appendix A.

3.4 Cyclic loading procedure

For each loading test one of the most important steps is to determine the loading regime. The regimen here is of a lateral reciprocal quasi-static loading, where the number of loading loops, load range, load frequency and load type are involved in each step and loading time. According to many studies the frame types and the seismic resistant systems' behavior must be tested according to ATC-24 protocol (1992). Here, the gradual increments prevail in this protocol. The focus of this protocol is on the frame behavior

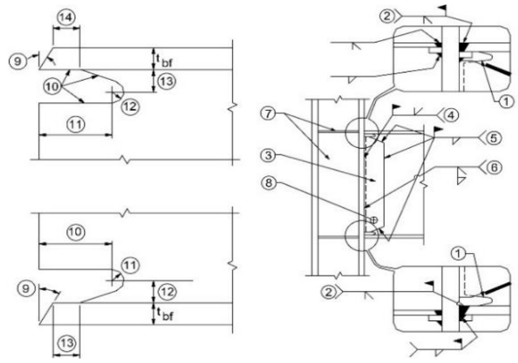

Fig. 11 WUF-W web connections and recommended weld access hole detail, FEMA-350 (2001)

within before and after yield range, and cover the frame fatigue in nonlinear behavior range by determining the minimum iteration count of cycles. In the elastic area, ⅓ and ⅔ of the amount of yield transfer are considered as the domain of the two primary cycles. The number of iteration of the three cycles in each load step consists of six, before the yield point. For yield point (δ_y) displacement and for following the three steps of loading after yield point, the number of three cycles are of concern, which end up in two.

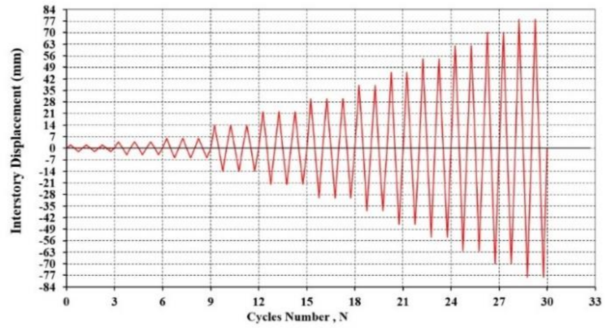

Fig. 12 The cyclic loading regime used in the reciprocating quasi-static test based on ATC-24, (1992)

Table 3 Hysteresis loading program

No.	Inter story Displacement (mm)	Cycles Number, N
1	± 2	3
2	± 4	3
3	± 6	3
4	± 14	3
5	± 22	3
6	± 30	3
7	± 38	2
8	± 46	2
9	± 54	2
10	± 62	2
11	± 70	2
12	± 78	2

This loading cycle remains constant after a peak deformation greater than δ_y. Fig. 12. The value of interstory displacement on the vertical axis versus the number of loading cycles are represented on the horizontal axis. In this figure, 78 *mm* displacement represents 5.1% drift. The hysteresis loading program are tabulated in Table 3.

All the run analyses and tests are of displacement-based control type and the inflicted load on the specimens follows a manner to obtain the cyclic loading protocol, Fig. 12.

4. Numerical analysis

4.1 Frame modelling

The objectives of this analyses consist of: 1) verifying the analytical models compared with the experimental results, 2) determining the shear capacity of the specimens at the end of the test, 3) predicting the specimen behavior, 4) estimating the load yield and the displacement level, 5) determining the specimens' location of the maximum stresses and strains in the elements for the installation of strain gauges and 6) applying the obtained results for the preliminary design.

For modeling and assessing the hysteretic behavior of all subject determines with respect to both the nonlinear geometric effects and materials, ABAQUS (2001) software is applied. For meshing and modeling of the boundary elements of the determine and elliptic brace, the elements of C3D8R (An8-node linear brick), are applied. Here the elements of beams, columns and elliptic bracing are 0.055 *m*, 0.055 *m* and 0.04 *m* in size, respectively. For meshing and modeling of filler plates in the frame corner, 4-node type 181 shell elements are applied with six degrees of freedom based on sensitivity analysis in order to reduce convergence problems. The out-of-plane movements of the models are limited. The initial defects in manufacturing phase of the determines are considered in the FEM, although the numerical models are recalibrated according to these experimental specimens. Validated FEM is one of useful tools for assessing the parameters.

The Von-Mises is applied in the models as the yield criterion. By applying the tensile test data on steel materials, a multi-linear kinematic hardening plasticity model is adopted to determine the ELBRFs' inelastic behavior. The initial geometrical imperfections, consisting of combined buckling modes, are introduced to the models through the IMPERFECTION option. The maximum imperfection value is 1 *mm*. The implicit solution method is selected based on Newark algorithm. Due to the strong nonlinearities caused by the local buckling of the boundary frames and the out-of-plane deformation of web planes, the implicit method initiates some convergence problems during repetition of Newton-Raphson. The explicit dynamic method is adopted as an effective tool for ELBRFs behavior analysis in order to overcome convergence problems in the repetition of Newton-Raphson.

4.2 Numerical analyses results

The seismic performance of ELBRF-E, ELBRF-B, ELBRF-1 & 2, SMRF and X-bracing systems is assessed during the reciprocating loading test. Some LVDTs are set along the loading axis on both sides of the specimen at different points on the columns to record the horizontal displacement level; some LVDTs are set perpendicular to the frame plate and in the place of the supports to record the occurrence of any in plane and out-of-plane deformations and buckling in the braces or uplift of the supports. The strain gauges are connected to the potential plastic areas of the specimen elements. The finite element results of the specimens consist of observations, hysteresis behaviors, strains, stresses, deformations, dissipated energy, etc. The analytical results are compared with that of the experimental results.

4.2.1 Stress and strain distributions and frame behavior

The outputs of the strain gauges indicate that in the SMRF specimen, the columns yield at their both ends and the stress value reaches its final value. The plastic hinges on both ends of the beam and columns occur due to their bending action. The Von-Mises stress contours in the final steps of loading is 62 *mm* displacement, that is, 4% drift, Fig. 13, where, the SMRF system forms an appropriate structural ductility under the lateral load, while in such a design, due to excessive relative displacement, caused by high structural flexibility and inevitable concentration stress at the ends of boundary elements and at the connection of beam-columns limit the SMRF application.

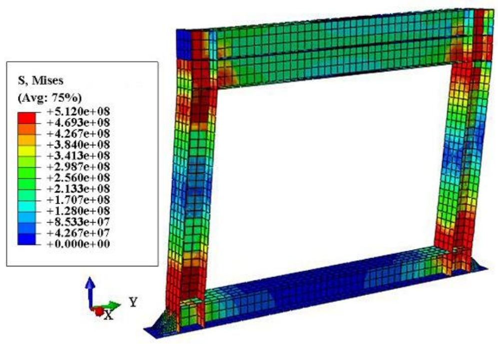

Fig. 13 SMRF, Von-Mises stress (Pa), at final load step

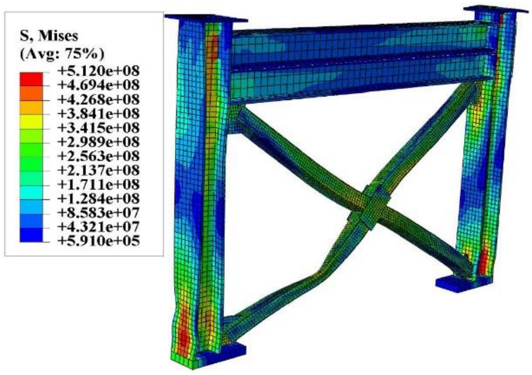

Fig. 14 X-Brace, Von-Mises stress (Pa), at final load step

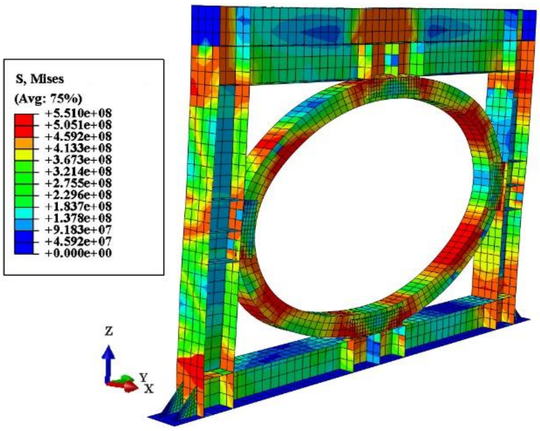

Fig. 15 ELBRF-E, Von-Mises stress (Pa), at final load step

The X-bracing system is of shear failure. The shear yield of this specimen is accompanied with a failure in the connection bay. Despite the maximum base shear strength, the high stiffness of this system, its ductility is significantly low due to the sudden buckling of braces and shear failure; therefore, the conventional buckling of braces, in addition to weakening compressive strength, indicate an unstable and asymmetric cyclic behavior during an earthquake. This asymmetric hysteretic response leads to loss of resistance due to post-buckling behavior, reduction of energy dissipation capacity, a significant difference between tensile and compressive strengths and a significant reduction in lateral stiffness. The value of stress at both ends of the beam and the column reaches the final value at the end of loading, where plastic hinges appear. The Von-Mises stress contours in the final steps of loading is 22 *mm* displacement, that is, 1.44% drift, Fig. 14, where, the stress at both ends of the beam and the column reaches the final value in the X-bracing system subject to the influence of the lateral load, at the final moment at very small displacement, thus appearance of plastic hinges.

In this newly proposed ELBRF-E bracing system, the stress values on the elliptical braces reached their final value, and no plasticity of the beams and columns is observed in the final loading step of 62 *mm* displacement, that is, 4.0% drift, Fig. 15. The strain contours in the final loading step are shown in Fig. 16.

In the ELBRF-B system, according to the output of the strain gauges, the values of critical strains on the elliptical brace and upper brackets are observed, and the stresses reach their final value. Plastic hinges are formed on the elliptical braces, and upper brackets at 54 *mm* displacement. There exists a direct relation between the lateral force and the lateral displacement. The upper area of the columns, both ends of the beam and its middle reach the maximum stress at the end of the 25^{th} cycle, at 62 *mm* displacement, that is, 4.0% drift, allowing the appearance of plastic hinges, consequently, the deformation inside the plane occurs in the upper part of the specimen.

In the ELBRF-1 & 2 systems, the plates are welded in the corners between the outer circumference of the elliptical braces and the internal flanges of the beam and column, which increase the stiffness of the system and the base shear strength. The stiffness of the ELBRF-2 system is slightly higher than that of the ELBRF-1 system due to thicker corners. Based on the records of the strain gauges' plastic hinges appear in the 7^{th} and 9^{th} cycles of the ELBRF-1 and ELBRF-2 specimens, respectively. As the lateral force increases, the lateral displacement of the frame increases as well, together with an increase in the appearance of plastic hinges on the elliptical braces and the plates in the corner.

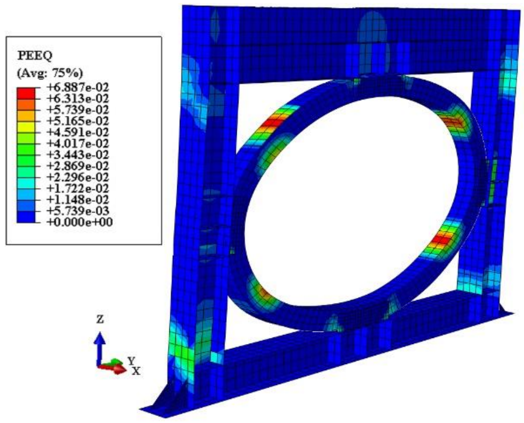

Fig. 16 ELBRF-E, Von-Mises strain (m/m), at final load step

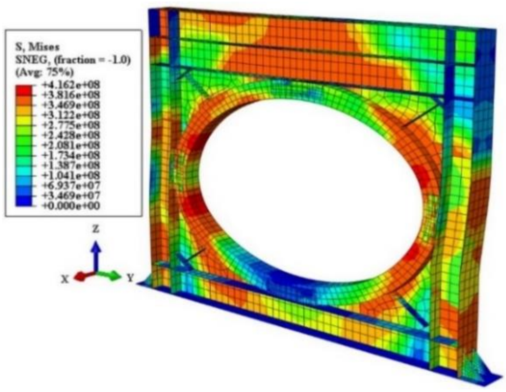

Fig. 17 ELBRF-1, Von-Mises stress (Pa), at final load step

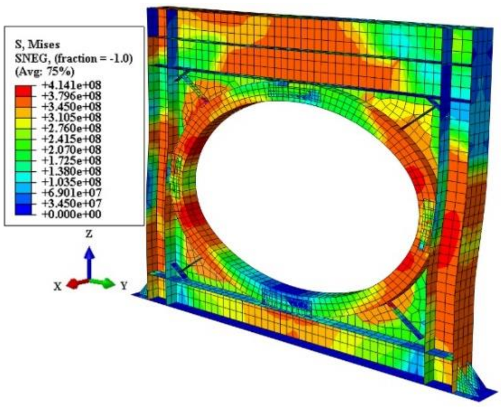

Fig. 18 ELBRF-2, Von-Mises stress (Pa), at final load step

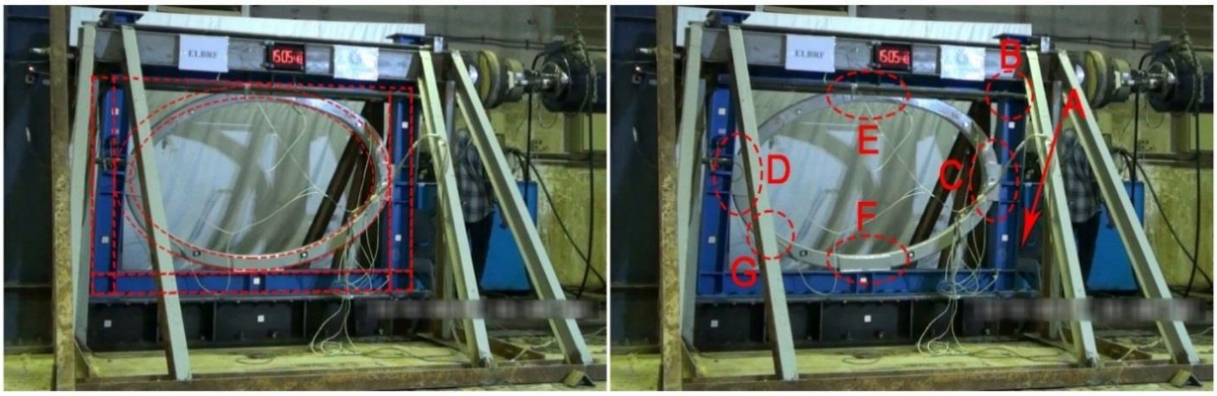

Fig. 19 ELBRF-E, at 5.1% drift, in cycle 30

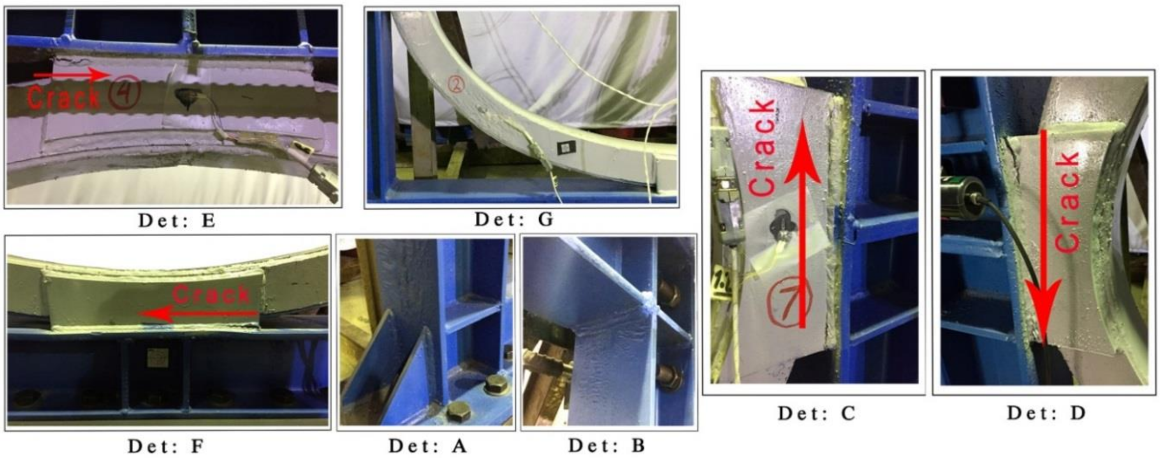

Fig. 20 The force transmission path from elliptic brace to beam and column, cracks in the welds and plastic areas at different points of the frame ELBRF-E

The values recorded by the strain gauges indicate that in ELBRF-1 and ELBRF-2, the middle region of the beam at the connection of the elliptical brace to the upper beam enter the plastic zone at the end of the 17^{th} and 19^{th} cycles, at 30 *mm* and 38 *mm* displacements, that is, 1.96% and 2.5% drifts, respectively. The presence of plates in the corners prevent column buckling and distortion at high shear strengths up to the 20^{th} cycle.

The Von-Mises stress contours of this newly proposed specimens at the 26^{th} cycle are shown is Figs. 17 and 18.

The maximum drift in structural design is within 2 or 3 %. In this experiment, the structural design in both the ELBRF-1 and ELBRF-2 is based on 5% drift, which allows the damage mechanism observation.

5. The test results and discussion

5.1 Frame behavior

5.1.1 SMRF test

The SMRF test remains linear by approximately 0.65% drift during the first 9 cycles of the test. The shear strengths of the frame are 443.1 kN, 485.6 kN and 507.8 kN at 14 *mm*, 22 *mm* and 38 *mm* displacements, that is, 0.915%, 1.44%, and 2.5% drifts, respectively. This specimen is resistant against the 4.0% drift; the test stops at the 25^{th} cycle. The shear capacity recorded in the stages of yielding and loading stoppage are 355.6 kN and 520.6 kN, respectively.

5.1.2 X-bracing test

The X-bracing test remains linear approximately at 0.14% drift during the first nine cycles of the test. By increasing the lateral displacement value, the crossed brace begins to buckle at its lower end. The test stops at the 15^{th} cycle. The recorded shear capacity of this system at the stages of yielding and loading stoppage are 504.3 kN and 866 kN, respectively.

5.1.3 ELBRF-E test

The ELBRF-E test remains linear approximately by 0.57% drift during the first 9 cycles of the test. The shear strengths of the frame are 1131.7 kN and 1179.1 kN in the 22 *mm* and 38 *mm* displacements, that is, 1.44%, 2.50% drifts, respectively. The lateral resistance of the system is on a rise, and reaches the horizontal load of 1210 kN of 3.53%

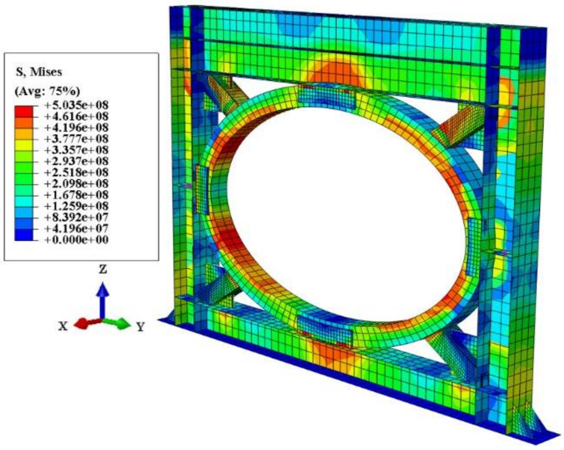

Fig. 21 ELBRF-B, deformation in FEM at 5.1% drift

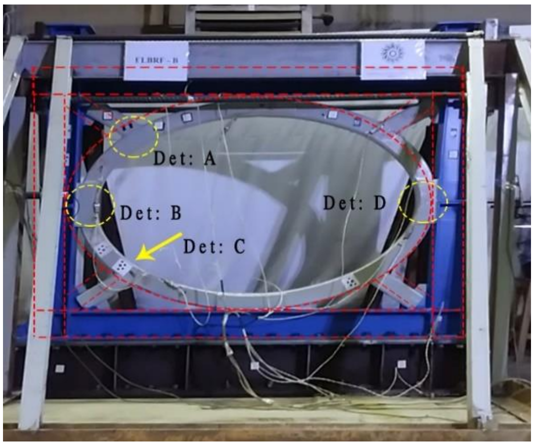

Fig. 22 ELBRF-B, deformation in test at 5.1% drift

drift and remains constant until the loading ends. The test stops at 30th cycle, and the recorded shear capacity in the stages of yielding, and loading stops at 791.5 kN and 1232 kN, respectively. The deformation of ELBRF-E bracing system at 30th cycle is an equivalent of 5.1% drift during the test, Fig. 19, where, the elliptical braces are deformed in the ELBRF-E bracing system subject to tensile and compressive strengths, with no buckling in the column. The elliptical shape of this bracing prevents the exertion of any axial force perpendicular to the vertical axis of the column. To assure more strength, applying auxiliary plates in the connections of the elliptical bracing to the beams and columns is contributive. The details of the force transmission path from elliptic brace to beam and column, cracks in the welds and plastic areas at different points of the specimen are shown in the final step of the test at 30th cycle at 5.1% drift, Fig. 20.

Lack of columns buckling during lateral loading in a manner that the smoothness of the columns is confirmed at all stages of the test, even in large displacements is the remarkable point in this bracing system. A change is observed in the elliptical bracing form as to cycles against tensile and compressive strengths. Another significant point in the behavior of this bracing system is the geometric shape, the curvatures of which at each stage of the change in the loading cycle direction, replaces the internal force of the braces from tension to compression and vice versa in a rapid manner and unlike linear braces prevents the out-of-plane buckling. This phenomenon indicates that the auxiliary plates at bracing to beam and column connection points is effective in preventing out-of-plain buckling.

5.1.4 ELBRF-B test

The ELBRF-B test is linear, approximately at 0.915% drift during the first 12 cycles of the test. The shear strengths of the frame are 1400 kN and 1430 kN, in the 30 *mm* and 38 mm displacements, that is, 1.96%, 2.50% drifts, respectively. The lateral resistance of the system is still on a rise, and it reaches the horizontal load of 1460 kN at 3.5% drift and remains constant until the loading ends. The test stops at 29th cycle. The shear capacity recorded at the yielding and loading end stages is 1280 kN and 1440 kN, respectively. Deformation of the ELBRF-B system at 29th cycle is an equivalent of 5.1% drift in the finite element output and test, Figs. 21 and 22, where, their comparison reveals a good agreement between the deformations in their numerical and experimental sense. The details of the force transmission path from elliptic brace to beam and column, cracks in the welds and plastic areas at different points of the frame are observed in the final step of the test in the 29th

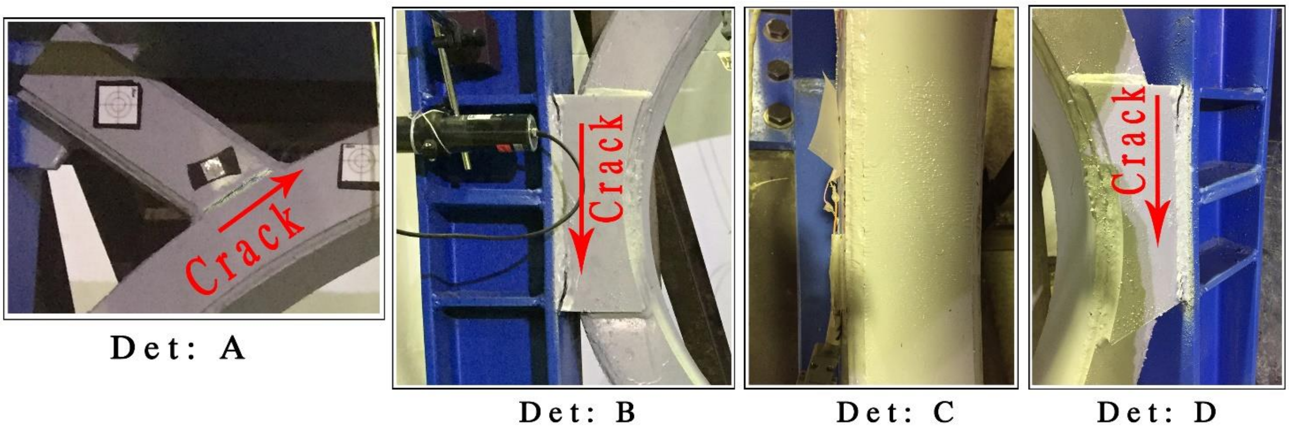

Fig. 23 The force transmission path from elliptic brace to beam and column, cracks in the welds and plastic areas at different points of the frame ELBRF-B

cycle is an equivalent of 5.1% drift, Fig. 23.

At the end of the 30th cycle, there is no buckling of the columns during lateral loading. A change is observed in the form the elliptical brace along the brackets in the reciprocating loading cycles. The behavior of this system due to its geographical shape is similar to that of the ELBRF-E system, where at each stage of loading cycle direction, the rapid replacement of the internal force of the braces change from tension to compression and vice versa occurs by opening or closing each quadrant of the elliptical brace.

This rapid change of the axial load in the elliptical brace in contrast to the linear braces, prevents out-of-plane buckling.

5.1.5 ELBRF-1 and ELBRF-2 tests

The ELBRF-1 and ELBRF-2 tests are linear, approximately by 0.33% drift (during the first 9 cycles). The ELBRF-1 shear strengths are 1672 kN, 1785 kN and 1830 kN, and the same for ELBRF-2, are 1518 kN, 1587 Kn and 1615 kN, with 14 *mm*, 30 *mm* and 46 *mm* displacements, that is, 0.915%, 1.96 % and 3.0% drifts, respectively.

By increasing the lateral load of the specimens, their lateral resistance increase in a sense that in both the ELBRF-1 and ELBRF-2, the horizontal load reaches 1847 kN and 1625 kN, respectively at 3.5% drift, and remains constant until the loading ends, and the test stops for both at 26th cycle.

The shear capacity recorded from the ELBRF -1 at yielding and loading stoppage is 1300 kN and 1860 kN, respectively, and the same for ELBRF -2, is 1240 kN and 1627 kN, respectively.

The deformation of the elliptical brace and distortion in the plates on the corner in the final cycles against tensile and compressive strengths are observed. Distortion and shrinkage on the plates are somewhat characterized by the scaling of their paint layer.

5.2 Hysteretic behaviour

The hysteretic curves drawn from experimental and analytical results are drawn according to the shear strength versus displacement of all the subject specimens and are assessed and compared together, Fig. 24. There exists an excellent agreement between the experimental and this numerical hysteresis curves. In general, the valuable information on hysteresis loops is collected from the structural systems. ELBRFs models indicate a good hysteretic behavior. In these curves it is observed that all specimens of the ELBRFs are of stable hysteretic behavior in the tensile regions.

All ELBRFs have elasticity, stable hysteresis loops, and high energy discharge capacity without destruction in boundary elements above 5% drift. In the hysteresis curves, stiffness deterioration is not observed in the ELBRFs. No buckling is observed during load excursions, which leads to the pinching phenomenon in hysteresis curves. This means that, applying this new elliptical brace in SMRF will result in a good performance of the system during cyclic loading, even at high resistance. Hysteresis loops indicate that there exists no significant reduction in the stiffness and strength in ELBRFs responses at high drifts. The cyclic envelop curves of all ELBRFs are drown in Fig. 25.

A quantitative comparison is run among the maximum strengths in numerical and experimental models of the subject specimens. In the experimental models, the maximum shear strength corresponding to the positive and negative drifts are marked on the hysteresis curves. The run tests exhibit higher values for resistance: 1.1% and more for positive drift and 1.15% more for negative drift in SMRF, 1.1% more for positive and negative drifts in X-bracing; 1.05% more for positive drift and 1.1% more for negative drift in the ELBRF-E, 1.1% more for positive drift and 1.05% more for negative drift in the ELBRF-B, 1.15% more for positive and negative drifts in the ELBRF-1, 1.12% more for positive and negative drifts in the ELBRF-2. By comparing the hysteresis curves, it can be deduced that the difference between the numerical and experimental models is slight.

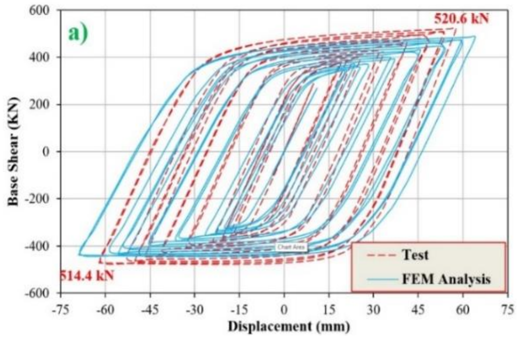

(a) SMRF specimen

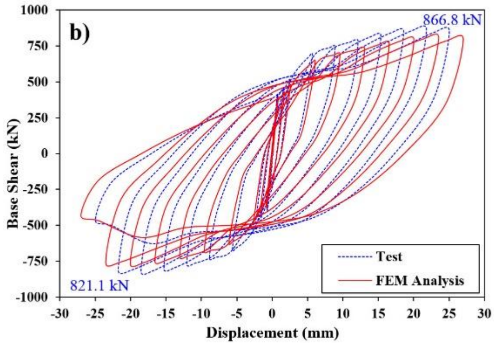

(b) X-Bracing specimen

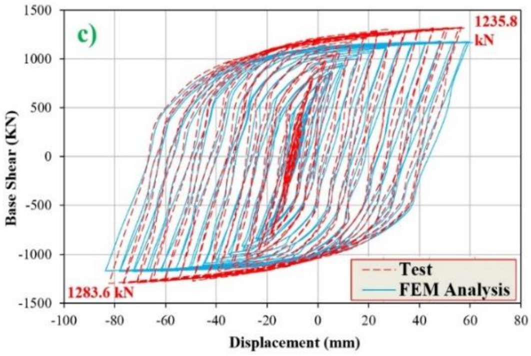

(c) ELBRF-E specimen

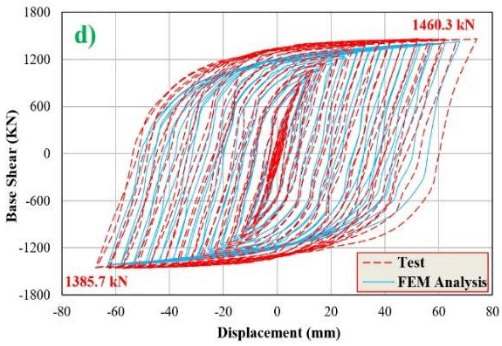

(d) ELBRF-B specimen

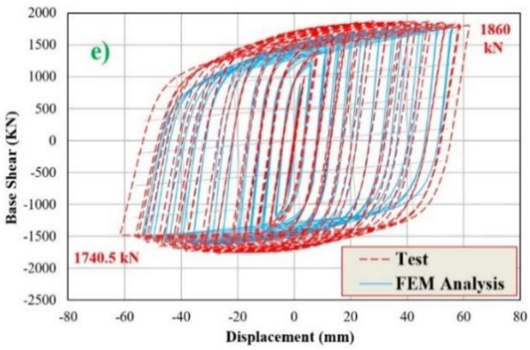

(a) ELBRF-1 specimen

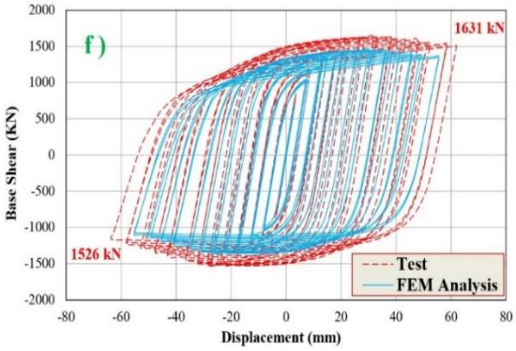

(b) ELBRF-2 specimen

Fig. 24 Hysteresis curves of the frames, from the tests

According to the hysteresis curves, the maximum shear strength SMRF, X-bracing, ELBRF-E, ELBRF-B, ELBRF-1 and ELBRF-2 is 520.62 kN, 866.83 kN, 1235.8 kN, 1460 kN, 1860 kN, and 1631 kN, respectively. The results indicate that applying ELBRF-E, ELBRF-B in the SMRF system increases the shear strength up to 2.36 and 2.80 time, respectively, indicating a significant energy dissipation in the ELBRF systems. The welded fillers at the corners of the ELBRF-1 and ELBRF-2 systems increase the shear strength of the system up to 1.50 and 1.32 time, respectively, in relation to ELBRF-E, indicating their high performance in tall buildings.

5.3 Dissipated energy

Energy dissipation is one of the main properties of a lateral resistant system subject to large cyclic loading in a sense that if the structural energy is absorbed and destroyed during the earthquake, the structure will undergo less damage (Xu *et al*. 2016, 2014). Energy dissipated by all the subject specimens is calculated and compared with one another. The region below the base shear-displacement curve represents the energy absorption of the structure. The cumulative energy dissipation of the specimens is calculated by the summation of the areas enclosed in the loops. The curves of dissipated energy in the specimens during the cyclic test are drawn in Fig. 26. By comparing the results, it is observed that the ELBRFs are capable of more energy dissipation than SMRF and X-bracing systems. The values of energy dissipated in the structural systems are bar-charted is in Fig. 27.

The energy dissipation capacity in the ELBRF-E system is 6 and 13 time higher than that of SMRF and X-bracing, respectively and in ELBRF-B system the same is 7.6 and 15 time.

Welded fillers at the corners of the ELBRF-1 and ELBRF-2 systems increase the energy dissipation capacity up to 28% and 10%, respectively, in relation to ELBRF-E.

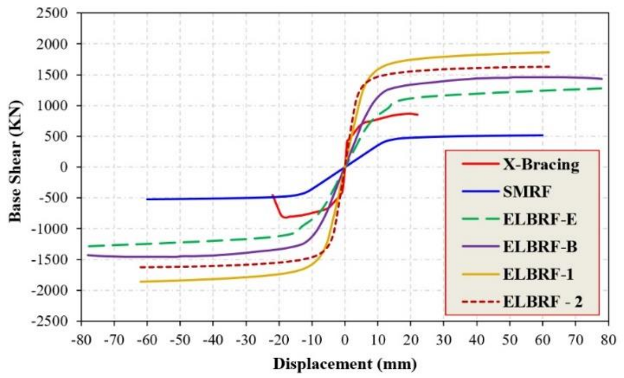

Fig. 25 Comparisons of the cyclic envelop curves of the tested specimens

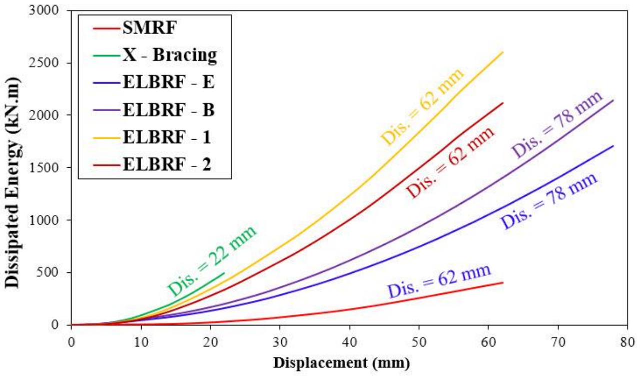

Fig. 26 The cumulative dissipated energies in the cyclic tests

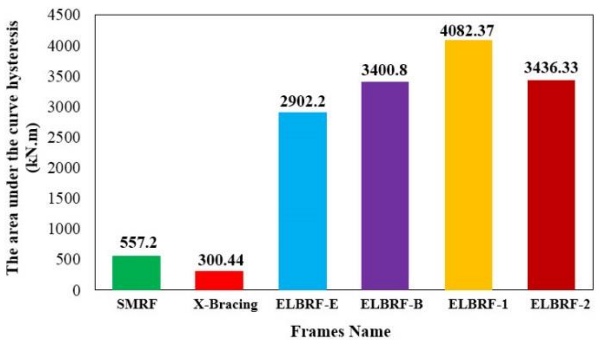

Fig. 27 Comparison of the results of hysteresis curve fulcrum

The X-bracing system is of a high elastic stiffness, while after reaching the yield point, the same is of a poor performance. The reason for the seismic energy absorption of the SMRF is the large lateral displacement, and the reason for the seismic energy absorption of ELBRF-E is the nonlinear activity of the elliptical brace and the formation of plastic hinges.

Although the SMRF is a good energy discharge system, while the transverse sections of its components may not be feasible in its economic sense. Structure stiffness is an effective factor in earthquakes, in addition to the importance of ductility and energy dissipation. The stiffness obtained from the structure behavior reduces the ductility and energy dissipation. Any structure must have proper stiffness and ductility. The ELBRF-1 & 2 specimens are stiffer than ELBRF-E systems due to the availability of the fillers at the corners of the frame.

6. Conclusions

In this article, for the first time, an experimental and numerical assessment is run on hysteretic behavior and energy dissipation capacity of four innovative single-story single-bay ELBRFs specimens at ½ scale under pseudo-static cyclic loading, which are compared with SMRF and X- Bracing in a single-story base model. The obtained results indicate that there exists a good agreement between experimental and theoretical results.

The general findings here are briefed as follows:

- This innovative ELBRFs as lateral resistant systems acting against lateral loads do not have the problem of architectural space in bracing systems in addition to improving structural behavior.
- The value of hysteretic energy in a structure is considered as an important criterion in the structure design and an important indicator of the degree of damage or its vulnerability, and is contributive in determining the structure behavior subject to seismic loads.
- The new ELBRFs consist of a combination of high ductility and energy dissipation capacity of SMRF and high elastic stiffness of CBF, which in addition to improving structural behavior, are cost efficient.
- Applying these new ELBRF-E and B systems lead to higher base shear absorption in relation to SMRF by 2.37 and 2.8 time, respectively. By adding the welded fillers at the corners of the ELBRF-E the maximum base shear capacity increases up to 1.4 time in average.
- The cyclic test results indicate that the ELBRFs systems are of stable hysteresis loops, and behave as a lateral loading systems of energy dissipation without any pinching, deterioration of stiffness and resistance in the envelope curve up to about 5% drift.
- The energy absorbed in ELBRFs systems is considerable, and it is more than that of the X-bracing and SMRF systems, which confirm its proper behavior against seismic loads. The energy absorbed in the ELBRF-E systems is about 5.2 and 9.6 times higher than that of X-bracing and SMRF systems, respectively; in ELBRF-B system, it is 6.1 and 11 times higher than that of SMRF and X-bracing systems, respectively. By adding the welded fillers at the corners of the ELBRF-E the energy absorption capacity increases up to 1.3 time in average.
- The formation of plastic hinges in ELBRFs systems in different specimens is introduced in the elliptical bracing, brackets and the welded plates at the corners. Appearance of the plastic hinges in the mentioned areas increase due to lateral force. Moreover, some specimens in the final cycles at high drifts, enter the plastic region at the mid-regions of the upper beam followed by the mid-regions of the column.
- In the ELBRFs, unlike SMRF and X-bracing systems, there exists a great distance between the relative deformation of the structure at yielding resistance and the

maximum relative deformation after entering the plastic zone, which leads to a discharge of more lateral loads. There exists a great distance between the formation of the first plastic hinge and when the structure collapses.

- The ELBRF-1 and ELBRF-2 systems are stiffer than the SMRF, ELBRF-E and ELBRF-B systems. Their ductility is slightly lower than that of ELBRF-E and ELBRF-B.
- The ELBRFs, due to the higher shear strength absorption, can be proposed as a practical solution for seismic load absorption in medium, tall and heavy structures.

Acknowledgments

This work is supported by the Shahid Rajaee Teacher Training University, (SRTTU). The support and assistance of the structural laboratory specialists are acknowledged and appreciated.

References

Abdollahzadeh, G., Faghihmaleki, H and Esmaili, H. (2018), "Comparing Hysteretic Energy and inter-story drift in steel frames with V-shaped brace under near and far fault earthquakes", *Alexandria Eng J.*, **57**(1), 301-308. https://doi.org/10.1016/j.aej.2016.09.015.

Abdollahzadeh, G. and Faghihmaleki, H. (2016), "Seismic-explosion riskbased robustness index of structures", *Int. J. Damage Mech.*, **26**(4), 1-18. https://doi.org/10.1177/1056789516651919.

AISC 360-10 (2010), Specification for Structural Steel Buildings, American Institute of Steel Construction, Chicago, IL.

Aguirre, J.J. and Almazán, J.L. (2015), "Demands potential reduction of optimally passive-controlled nonlinear structures", *J. Eng. Struct.*, **89**(15), 130-146. https://doi.org/10.1016/j.engstruct.2015.01.009.

Applied Technology Council (1992), Guidelines for cyclic seismic testing of component of steel structures. Redwood City, CA: ATC-24.

ASTM A 370-05. (2005), Test methods and definitions for mechanical testing of steel products, Am. Soc. Test Mater., 1-47.

Aristizabal-Ochoa, J. D. (1986), "Disposable knee bracing: improvement in seismic design of steel frames", *J. Struct. Eng.-ASCE*, **112**(7), 1544-1552. ttps://doi.org/10.1061/(ASCE)0733-9445(1986)112:7(1544).

Bayat, M. and Bayat, M. (2014), "Seismic behavior of special moment-resisting frames with energy dissipating devices under near source ground motions", *Steel Compos. Struct.*, **16**(5), 533-557. https://doi.org/10.12989/scs.2014.16.5.533.

Benavent, A. (2007), "An energy-based damage model for seismic response of steel structures", *Earthq. Eng. Struct. D.*, **36**, 1049-1064. https://doi.org/10.1002/eqe.671.

Black, C.J., Makris, N. and Aiken, I.D. (2004), "Component testing, seismic evaluation and characterization of buckling-restrained braces", *J. Struct Eng.*, **130**(6). https://doi.org/10.1061/(ASCE)0733-9445(2004)130:6(880).

Bojórquez, E., Astorga, L., Reyes-Salazar, A., Terán-Gilmore, A., Velázquez, J., Bojórquez, J. and Rivera, L. (2015), "Prediction of hysteretic energy demands in steel frames using vector-valued IMs", *Steel Compos. Struct.*, **19**(3), 697-711. https://doi.org/10.12989/scs.2015.19.3.697.

Cao, H. and Friswell, M.I. (2009), "The effect of energy concentration of earthquake ground motion on the nonlinear response of RC Structures", *Soil Dyn. Earth. Eng.*, **29**(2), 292–299. https://doi.org/10.1016/j.soildyn.2008.02.003.

Christopoulos, C., Tremblay, R., Kim, H.J. and Lacerte, M. (2008), "Self-centering energy dissipative bracing system for the seismic resistance of structures: Development and validation", *J. Struct Eng.*, **134**(1). https://doi.org/10.1061/(ASCE)0733-9445(2008)134:1(96).

Doğru, S., Akşar, B., Akbaş, B. and Shen, J. (2017), "Parametric study on energy demands for steel special concentrically braced frames", *Steel Compos. Struct.*, **24**(2), 265-276. https://doi.org/10.12989/scs.2017.24.2.265.

Engelhardt, M.D. and Popov, E.P. (1989), "On design of eccentrically braced frames", *Earth. Spectra*, **5**(3), 495-511. https://doi.org/10.1193/1.1585537.

Fanaie, N., Aghajani, S. and Afsar Dizaj, E. (2016), "Strengthening of moment-resisting frame using cable–cylinder bracing", *J. Adv. Struct.Eng.*, **19**(11), 1-19. https://doi.org/10.1177/1369433216649382.

Fanaie, N. and Ezzatshoar, A. (2014), "Studying the seismic behavior of gate braced frames by incremental dynamic analysis (IDA)", *J. Constr. Steel Res.*, **99**, 111-120. *https://doi.org/10.1016/j.jcsr.2014.04.008.*

Fanaie, N. and Shamlou, S.O. (2015), "Response modification factor of mixed structures", *Steel Compos. Struct.*, **19**(6), 1449-1466. : http://dx.doi.org/10.12989/scs.2015.19.6.1449.

Fanaie, N., Dizaj, E.A. and Zarifpour, A. (2017), "Probabilistic seismic demand of steel frames braced with reduced yielding segment buckling restrained braces", *J. Adv. Struct. Eng.*, **21**(7), 1-19. https://doi.org/10.1177/1369433217737115.

FEMA (2000), American Society of Civil Engineers. Prestandard and commentary for the seismic rehabilitation of buildings, Washington (DC): Federal Emergency Management Agency No.356.

FEMA (2001), Seismic design criteria for new moment-resisting steel frame construction, Federal Emergency Management Agency Report No. 350.

Goel, S.C. and Berg, G.V. (1968), "Inelastic earthquake response of tall steel frames", *J. Struct. Div.- ASCE*, **94**(8), 1772-1907.

Hibbitt, Karlsson, & Sorenson, Inc., (HKS). (2001), ABAQUS/Explicit User's Manual. Version 6.2, Hibbitt, Karlsson, & Sorenson Inc., Pawtucket, Rhode Island.

Housner, G.W. (1956), "Limit design of structures to resist earthquake", *Proceedings of the 1st World Conference on Earth. Eng.*, Berkeley, California.

Housner, G.W. and Jennings, P.C. (1977), "The capacity of extreme earthquake motions to damage structures", Structural and geotechnical mechanics, Inc., Englewood Cliffs, N.J., 102-116.

Kaveh, A., Farahmand Azar, F., Hadidi, A., Rezazadeh Sorochi, F. and Talatahari, S. (2010), "Performance-based seismic design of steel frames using ant colony optimization", *Constr. Steel Res.*, **66**, 566_574.

Kazantzi, A.K., Vamvatsikos, D. and Lignos, D.G. (2014), "Seismic perpormance of a steel moment resisting frame subject to strength and ductility uncertainty", *Eng Struct.*, **78**(1), 69-77. https://doi.org/10.1016/j.engstruct.2014.06.044.

Khaloo, A., Nozhati, S., Masoomi, M. and Faghihmaleki, H. (2016), "Influence of earthquake record truncation on fragility curves of RC frames with different damage indices", *J. Build. Eng.*, 7, 23-30. https://doi.org/10.1016/j.jobe.2016.05.003.

Khatamirad, M. and Shariatmadar, H. (2017), "Experimental and analytical study of steel slit shear wall", *Steel Compos. Struct.*, **24**(6), 741-751. https://doi.org/10.12989/scs.2017.24.6.741.

Kunnath, S.K. and Chai, Y.H. (2004), "Cumulative damage-based inelastic cyclic demand spectrum", *Earthq. Eng. Struct. D.*, **33**, 499-520. https://doi.org/10.1002/eqe.363.

Kuwamura, H. and Galambos, T.V. (1989), "Earthquake load for structural reliability", *J. Struct. Eng. - ASCE*, **115**(6), 1446-1462. https://doi.org/10.1061/(ASCE)0733-9445(1989)115:6(1446).

Leger, P. Member, ASCE, and Dussault, S. (1992), "Seismic-energy dissipation in MDOF structures", *J. Struct. Eng.*, **118**, 1251-1269. https://doi.org/10.1061/(ASCE)0733-9445(1992)118:5(1251).

López-Barraza, A., Ruiz, S.E., Reyes-Salazar, A. and Bojórquez, E. (2016), "Demands and distribution of hysteretic energy in moment resistant self-centering steel frames", *Steel Compos. Struct.*, **20**(5), 1155-1171. https://doi.org/10.12989/scs.2016.20.5.1155.

Lubell, A.S. (1997), "Performance of un-stiffened steel plate shear walls under cyclic quasi-static loading", M.Sc. Thesis. Vancouver, BC, Canada: Department of Civil Engineering University of British Columbia; 1997.

Mofid, M. and Khosravi, P. (2000), "Non-linear analysis of disposable knee bracing", *Comput. Struct*., **75(1)**, 65-72. https://doi.org/10.1016/S0045-7949(99)00085-1.

Okazaki, T., Arce, G., Ryu, G. and Engelhardt, M.D. (2004), "Recent research on link performance in steel eccentrically braced frames", *Proceedings of the 13th world conference on Earth. Eng.,* Canada.

Richards, P.W. and Uang, C.M. (2005), "Effect of flange width-thickness ratio on eccentrically braced frame link cyclic rotation capacity", *Struct. Eng*., **131**(10), 1546-1552. https://doi.org/10.1061/(ASCE)0733-9445(2005)131:10(1546).

Richards, P.W. and Uang C.M. (2006), "Testing protocol for short links in eccentrically braced frames", *Struct. Eng*., **132**(8), 1183-1191. https://doi.org/10.1061/(ASCE)0733-9445(2006)132:8(1183).

Roeder, C.W. and Popov, E.P. (1978a), "Eccentrically braced frames for earthquakes", *J. Struct. Div. Am. Soc. Civil Eng*., **104** (3), 391-412.

Sahoo, D.R. and Chao, S.H. (2010), "Performance-based plastic design method for buckling-restrained braced frames", *Eng. Struct*., **32**(9), 2950-2958. https://doi.org/10.1016/j.engstruct.2010.05.014.

Shin, D.H. and Kim H.J., (2016) "Influential properties of hysteretic energy dissipating devices on collapse capacities of frames", *Constr. Steel Res*., **123**, 93-105. https://doi.org/10.1016/j.jcsr.2016.04.022.

Speicher, M.S. and Harris, J.L. (2016), "Collapse prevention seismic performance assessment of new special concentrically braced frames using ASCE 41", *Eng. Struct*., **126**(1), 652-666. https://doi.org/10.1016/j.engstruct.2016.07.064.

Sultana, P. and Youssef, M.A. (2016), "Prediction of local seismic damage in steel moment resisting frames", *Constr. Steel Res*., **122**, 122-137. https://doi.org/10.1016/j.jcsr.2016.03.011.

Taniguchi, M. and Takewaki, I. (2015), "Bound of earthquake input energy to building structure considering shallow and deep ground uncertainties", *Soil Dyn. Earthq. Eng*., **77**, 267-273. https://doi.org/10.1016/j.soildyn.2015.05.011.

Uang, C.M. and Bertero, V.V. (1998), "Implication of recorded earthquake ground motion on seismic design of buildings structures", Report no. UBC/EERC-88/13, Earth. Eng. Research Center, University of California, Berkeley.

Wu, J. and Hanson, R.D. (1989), "Study of inelastic spectra with high damping", *J. Struct. Eng.- ASCE*, **115**(6), 1412-1431. https://doi.org/10.1061/(ASCE)0733-9445(1989)115:6(1412).

Xu, L.H.., Fan, X., Lu, D.C. and. Li, Z. (2016), "Hysteretic behavior studies of self-centering energy dissipation bracing system", *Steel Compos. Struct*., **20**(6), 697-711. https://doi.org/10.12989/scs.2016.20.6.697.

Xu, L.H.. Li, Z. and Lv, Y. (2014), "Nonlinear seismic damage control of steel frame-steel plate shear wall structures using MR dampers", *Earthq. Struct*., **7**(6), 937-953. https://doi.org/10.12989/eas.2014.7.6.937..

Xu, L.H., Xie, X.S. and Li, Z.X.. (2018), "Development and experimental study of a self-centering variable damping energy dissipation brace", *Eng Struct*., **160**(1), 270-280. https://doi.org/10.1016/j.engstruct.2018.01.051.

Xu, L.H., Fan, X.W. and Li, Z.X.. (2018), "Cyclic behavior and failure mechanism of self-centering energy dissipation braces with pre-pressed combination disc springs", *J. Earth. Eng. Struct. D.*, **46**(7), 1065-1080. https://doi.org/10.1002/eqe.2844.

Xu, L.H., Xie, X.S. and Li, Z.X. (2018), "A self-centering brace with superior energy dissipation capability: development and experimental study", *Smart Mater. Struct.*, **27**(9).

Xue, W., Yang, F. and Li, L. (2009), "Experiment research on seismic performance of prestressed steel reinforced high performance concrete beams", *Steel Compos. Struct*., **9**(2), https://doi.org/10.12989/scs.2009.9.2.159.

Zahrah, T.F. and Hall, W.J. (1984), "Earthquake energy absorption in SDOF structures", *J. Struct. Eng*., **110**(8), 1757-1772. https://doi.org/10.1061/(ASCE)0733-9445(1984)110:8(1757).

CC

Appendix A

1) Weld access hole, see Fig. 7(b).
2) CJP groove weld at top and bottom flanges: at the top flange, either i) backgouge is removed to be replaced by 8mm minimum fillet weld, or ii) 8 *mm* fillet weld is added without backgouge removed. At bottom flange, backgouge is removed to be replaced by 8 *mm* minimum fillet weld. Weld: QC/QA Category AH/T.
3) Tab of thickness equals to that of the beam web. Shear tab length shall be so as to allow 6mm overlap with the weld access hole at the top and bottom, and the width shall extend 50 *mm* minimum back along the beam, beyond the end of the weld access hole.
4) CJP groove weld full length of web between weld access holes. Provide non-fusible weld tabs. Remove weld tabs after welding and grind end of weld smooth at weld access hole. Weld: QC/QA Category BH/T.
5) Fillet weld shear tab to beam web. Weld size shall be equal to the thickness of the shear tab minus 1.5 *mm*. Weld shall extend over the top and bottom one-third of the shear tab height and across the top and bottom. Weld: QC/QA Category BL/L.
6) Full-depth partial penetration from far side. Weld: QC/QA Category BM/T.
7) continuity plates and web double plate.
8) Erection bolts: number, type, and size selected for erection loads. Note, not applied here.
9) Larger of t_{bf} or 12 *mm*. (plus ½ t_{bf}, or minus ¼ t_{bf}).
10) Bevel as required by AWSD 1.1 for selected groove weld procedure.
11) 10 *mm* minimum radius (plus not limited, or minus 0).
12) ¾ t_{bf} to t_{bf}, 19 *mm* minimum (– 6 *mm*).
13) See FEMA-353, Recommended Specifications and Quality Assurance Guidelines for Steel Moment-Frame Construction for Seismic Applications, for fabrication details including cutting methods and smoothness requirements.
14) 3 t_{bf}. (– 12 *mm*).